Supplementary Materials:
Eavesdropping by the edge supercurrent on blockade correlation between competing condensates in a Weyl superconductor

Stephan Kim[1,2], Shiming Lei[3], Leslie M. Schoop[3], R. J. Cava[3], and N. P. Ong[1,§]

Departments of Physics[1], Electrical and Computer Engineering[2] and Chemistry[3], Princeton University, Princeton, NJ 08544, USA

(Dated: September 6, 2022)

I. ADDITIONAL ANALYSES OF DEVICES

A. Categorization of samples

Table S1 lists the parameters of the 8 $MoTe_2$ devices used in the experiment. The five devices SA, SB, SI, SJ and SK (flagged by an asterisk *) are in the parallel-strip electrodes with link lengths $\ell_1 = \ell_2 = d < \lambda$. They all show the group II signatures associated with edge states at the links (strong oscillations in $(dV/dI)_0$, antihysteresis and transition $(dV/dI)_0 \to 0$ occuring at relatively large B (30–90 mT). The amplitudes and/or field scales of these features are monotonically suppressed as the separation d is increased from 156 nm (in SA) to 703 nm (SB).

In devices SH, SD and SF the Nb contacts cover a contact area much smaller than the physical area of the crystal ($L_c \ll \ell_1, \ell_2$). Because of the long link lengths ℓ_1 and ℓ_2 ($\gg \lambda$) the Nb pair field decays before the edge supercurrents can form a closed loop. Hence the group II features are absent. Even when one of the links is shorter than λ, these features do not appear. Thus in device SF, which has $\ell_1 < \lambda$ but $\ell_2 \gg \lambda$, the group II features are absent. Again this shows that supercurrents in both links are necessary to close the loop (SF is discussed further below).

B. Flux focusing effect

Figure S1 shows a typical setup of a parallel-strip device. For such devices, the well-known flux focussing effect enhances the flux density B within the slit area well above the external (applied) flux density $B_{ext} = \mu_0 H$. This arises because flux expulsion from adjacent Nb strips forces the flux lines to concentrate inside the slit area. This effect affects all devices with the parallel-strip geometry, in a consistent way. The measured period ΔB of $(dV/dI)_0$ differed from the values ΔB_0 calculated from the flux $B_{ext}\mathcal{A}_\phi$.

In general, the quantization area $\mathcal{A}_\phi$ is related to the observed period ΔB by

$$\Delta B = \phi_0/\mathcal{A}_\phi. \tag{S1}$$

Using this expression, we infer an area $\mathcal{A}_\phi$ that is far too large (shown as dotted lines in Fig. S1). The penetration length into the Nb strip W_f (see Fig. S1) is given roughly by

$$2W_\mathrm{f} + d \simeq \frac{2\phi_0}{w\Delta B}, \tag{S2}$$

where we approximate the flux in Nb as uniform. In Table S1 we show that the ratio $W_\mathrm{f}/W_\mathrm{e}$ is 0.34 to 0.39.

C. Decay length λ along edge

The decay length λ, which governs the decay of the pair field $\hat{\eta}$ along a link, is best estimated from the differential resistance color maps. From the full color maps, the values of $\mu_0 H_{\mathrm{osc}}^{\mathrm{max}}$ were obtained, which are the magnetic fields at which the oscillations of the critical current become unresolved. At this field, the proximity effect of the niobium pair field $\hat{\eta}$ on the edge mode is undetectable. Figure S3 shows the initial steep decrease of

Device	spacing d	w	link ℓ_1	link ℓ_2	ΔB_0	ΔB	$W_\mathrm{f}/W_\mathrm{e}$	$I_{\mathrm{c,max}}$
units	nm	nm	nm	nm	mT	mT	–	μA
SA*	156	3,820	156	156	6.40	0.955	0.344	80
SB*	703	3,180	703	703	1.85	0.80	0.35	5
SD	810	1,400	8,030	17,670	-	-		15
SF	764	7,580	764	11,400	-	-		23
SH	1,240	1,340	5,420	5,710	-	-		21
SI*	285	3,380	285	285	4.29	0.90	0.39	15
SJ*	634	3,420	634	634	1.91	0.80	0.33	10
SK*	197	7,420	197	197	2.83	0.44	0.39	–

TABLE S1. Parameters of the 8 devices used in the experiment. For devices in the parallel-strip geometry (indicated by the asterisk *), the period ΔB is given by Eq. S1.

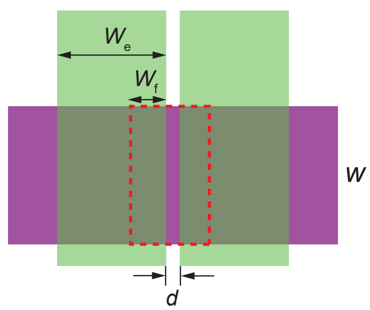

FIG. S1. Sketch of parallel-strip device. The purple rectangle represents the exfoliated $MoTe_2$ crystal, green rectangles are deposited niobium electrodes. The red dotted line outlines the area $\mathcal{A}_\phi$ inferred from the observed period (Eq. S1). The link lengths ℓ_1 and ℓ_2 equal d.

$\mu_0 H_{\mathrm{osc}}^{\mathrm{max}}$ vs. d. However, at large d (700 nm), it asymptotes to a much slower trend instead of exponentially decaying to zero. The solid curves are fits to

$$B_{\mathrm{osc}}^{\mathrm{max}} = A_1 \mathrm{e}^{-d/\lambda_a} + A_2, \tag{S3}$$

where A_1 and A_2 are constants. As an approximation, we may identify λ with λ_a ($\sim$250 nm). However, this seriously underestimates the non-exponential decay. The oscillations are observable to $H \simeq 30$ mT for devices with $d = 700$ nm. The reason for the persistence of the edge supercurrent at large d is a very interesting effect that is under further investigation.

D. Phase slippage and phase rigidity at links

Here we comment on what happens when the links transition to a finite-resistance state. Close inspection of the color maps in Figs. 1B and 1C (main text) shows that the edge oscillations (which we identify with the links) remain well-resolved even when the differential resistance dV/dI is finite (yellow on the color scale). Similarly, in Figs. 3E and 3F, the periodic oscillations remain sharply resolved when $(dV/dI)_0$ becomes finite. As we have argued, the oscillations reflect successive fluxoid entry into the area $\mathcal{A}_\phi$. At first glance, it may seem puzzling that the edge condensate at the links retains sufficient phase rigidity to "count" individual fluxoids when dV/dI (or $(dV/dI)_0$) is driven to finite values by increasing I (in the case of dV/dI in the color map) or increasing H (in the case of $(dV/dI)_0$). The resolution comes from the 1D nature of the edge condensate. We argue that the edge supercurrent at the links displays a finite voltage because of rapid successive nucleation of phase slips at weak spots (possibly at the interface between a link and a segment under Nb). The local vanishing of the edge condensate amplitude at a weak spot allows the phase to jump by 2π, but phase rigidity holds away from the weak spot. Hence a finite voltage across the links does not imply loss of phase rigidity in the edge condensate. The color maps in Figs. 1B and 1C show directly that the edge condensate is still rigid despite the finite value of dV/dI.

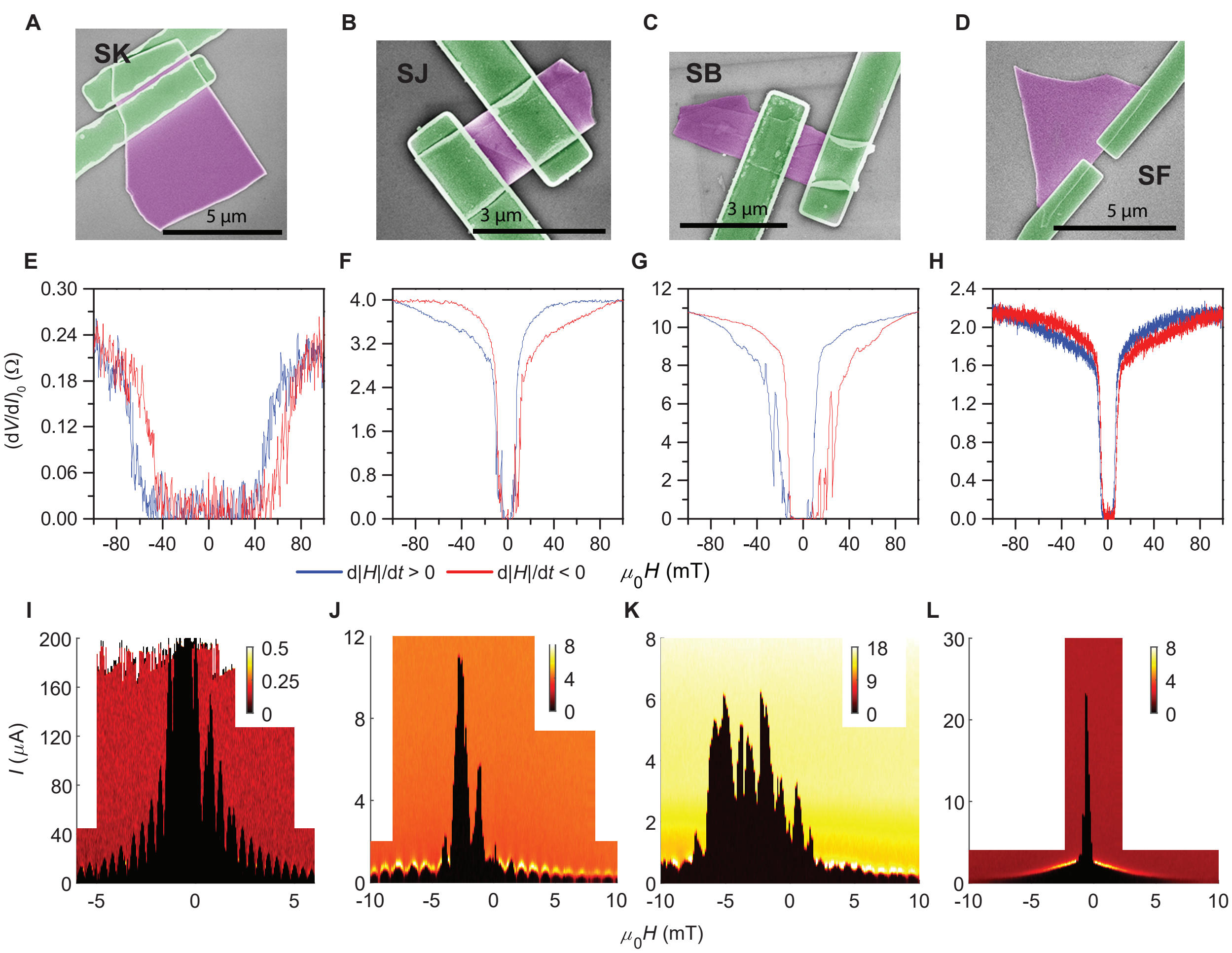

FIG. S2. False color SEM images (A-D), anti-hysteresis (E-H), and dV/dI vs. H (I-L) of four devices (SK, SJ, SB, and SF). Panel A shows the SEM image of SK, Panel B for SJ, Panel C for SB, and Panel D for SF, respectively. Data from the same column are from the same device, i.e. Panel E and Panel I are from SK in Panel A.

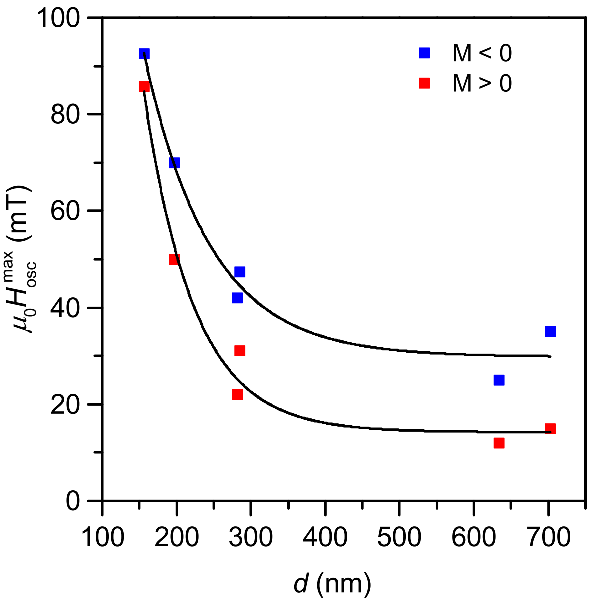

FIG. S3. The value $H_{\mathrm{osc}}^{\mathrm{max}}$ with respect to d. Blue and red symbols are for in-bound and out-bound branches, respectively.

II. STOCHASTIC SWITCHING OF BULK CRITICAL CURRENT

To investigate the stochastic switching of critical current, the critical current I_{c} of device of interest was considered as a random variable, and it was sampled at different applied magnetic fields. The differential resistance measurement procedures in Methods of main text were repeated for a total of $N = 100$ times on the device of interest at a given field. For the n^{th} sampling run, the realization I_n of random variable $I_{\mathrm{c},n}$ satisfied $dV/dI(I_n) = \frac{1}{2}\big((dV/dI)_N - (dV/dI)_S\big)$, where $(dV/dI)_N$ was the differential resistance of normal state and $(dV/dI)_S$ that of superconducting state. The collected data were interpolated with $M = 3,000$ points, which were orders of magnitude larger than the number of actual data points, for a higher resolution of I_n. At a fixed value of H, the mean of I_{c} and its standard deviation s were calculated from the set of N measurements $\{I_{\mathrm{c},n}\}$ as

$$\langle I_{\mathrm{c}} \rangle = \frac{1}{N} \sum_n I_{\mathrm{c},n}, \quad s^2 = \frac{1}{N} \sum_n (I_{\mathrm{c},n} - \langle I_{\mathrm{c}} \rangle)^2. \tag{S4}$$

Using the distribution function $\mathcal{P}(I)$, we may express the mean as

$$\langle I_{\mathrm{c}} \rangle = \int I \, \mathcal{P}(I_{\mathrm{c}} = I) dI. \tag{S5}$$

The square of the standard deviation is

$$s^2 = \int (I - \langle I_{\mathrm{c}} \rangle)^2 \, \mathcal{P}(I_{\mathrm{c}} = I) dI. \tag{S6}$$

The cumulative distribution function $F_{I_{\mathrm{c}}}(I)$ of I_{c} reveals a complementary way to see the bimodal nature of the distribution of switching current, discussed in Fig. 3b of main text.

The function $F_{I_c}(I)$ is defined as $F_{I_c}(I) = \mathcal{P}(I_c \leq I) = \frac{1}{N}\sum_n^N \mathbf{1}_{I_{c,n}\leq I}$. Figure S5 shows $F_{I_c}(I)$ of SC and SJ. The profile of F_{I_c} is similar to a step function at large H, showing one large jump from $F_{I_c} = 0$ to $F_{I_c} = 1$. In this field regime, either $\hat{\eta}$ or $\hat{\psi}$ dominated the supercurrent, resulting in nearly identical values of realization of I_c. In the presence of competition, especially near the shifted central lobes ($\mu_0 H = -2.5$ mT for SC and $\mu_0 H = -3$ mT for SJ), two major transitions are observed. For SC at $\mu_0 H = -2.5$ mT, a bunch of I_c is located around $I \sim 9$ μA and the other around $I \sim 11$ μA. Simliarly, there is one at $I \sim 6$ μA and the other at $I \sim 8$ μA for SJ at $\mu_0 H = -3$ mT. The two discrete sets of jumps in F_{I_c} imply that the distribution of I_c is dominated by two modes.

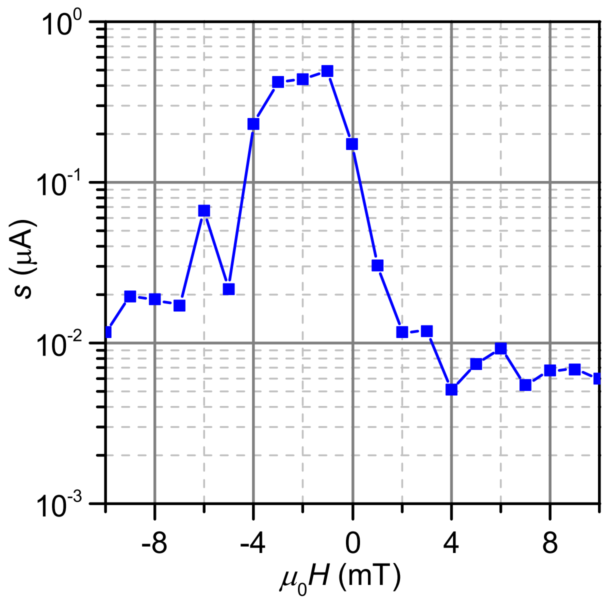

FIG. S4. The sample standard deviation s of I_c with respect to the applied field for SJ. Similar to the data presented in Fig. 2 of main text, s increased by more than an order of magnitude at small fields, when both niobium and intrinsic bulk $MoTe_2$ were present.

III. PHASE-NOISE ANALYSIS OF CRITICAL CURRENT OSCILLATIONS

A. Phase of edge oscillations vs. field

In a magnetic field H, the phase $\theta(H)$ of the edge oscillation is inferred from the scalloped field profile of the critical current $I_c(H)$ [1] as follows. The periodic modulation of critical current is

$$\frac{\Delta I_c}{Ic} \sim \left(n - \frac{\phi}{\phi_0}\right)^2, \qquad \left(n - \frac{1}{2} < \frac{\phi}{\phi_0} < n + \frac{1}{2}\right), \tag{S7}$$

where n is an integer, ϕ the flux, and $\oint \nabla\theta \cdot d\vec{\ell} = 2\pi n$ due to fluxoid quantization. The entrance of a flux quantum implies a total phase winding of 2π, which appears as a complete lobe of the scalloped profile.

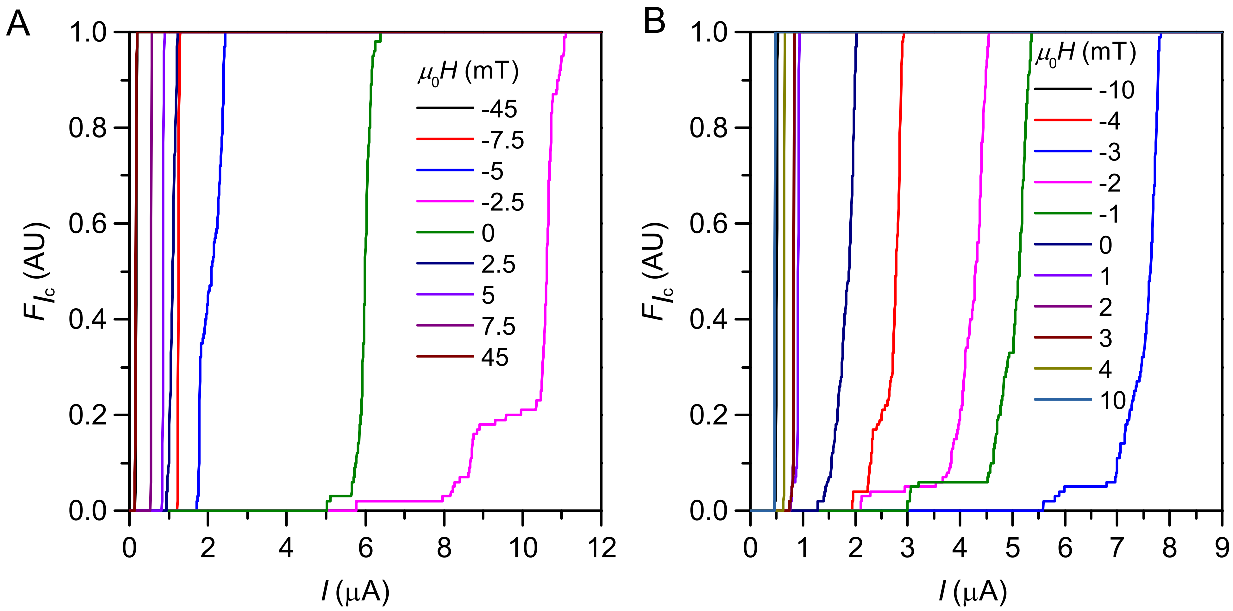

FIG. S5. The cumulative distribution function $F_{I_c}(I)$ of SC in panel A and SJ in panel B.

For the m^{th} lobe, we define θ to be $2\pi(m-1)$ and $2\pi m$ at the two cuspy minima bracketing the lobe. At the maximum in I_c, the phase is $2\pi(m-\frac{1}{2})$ (see blue lines in Fig. S6). Fixing the phase at the three points allows us to linearly interpolate θ over the lobe.

The phase noise is comprised of discrete jumps $\delta\theta$ as well as gradual drift of the period. For lobes with a single jump, θ can still be smoothly interpolated from either minimum (with a discontinuity at the jump). When both mimima are obscured because of multiple jumps, we extrapolate the curves from the two neighboring lobes. Using this procedure, we extract the field dependence of the phase $\theta(H)$ from the field profile of dV/dI. This is plotted as the solid blue curve in Fig. S7.

In the absence of phase noise, the ideal phase has the form

$$\theta_0(\Delta B, H) = 2\pi(H - H_0)/\Delta B, \tag{S8}$$

where the period ΔB and the start field H_0 are empirically determined.

B. Quantifying the phase noise

The competition between the pair field $\hat{\eta}$ from niobium and the intrinsic field $\hat{\psi}$ in $MoTe_2$ results in stochasticity in the edge oscillations, especially visible on in-bound branches (with $d|H|/dt < 0$). The noise appears mainly as phase fluctuations, but amplitude fluctuations contribute as well when oscillations are strongly chaotic. Our focus is on the phase noise which we quantify by comparing the observed phase $\theta(H)$ against the ideal (noise-free) oscillation $\theta_0(H)$ given in Eq. S8. We define the deviation

$$\Delta\theta(H) = \theta(H) - \theta_0(\Delta B, H) \tag{S9}$$

where ΔB is the period. To find the optimal ΔB, we use the interval on the out-bound branch $15 < \mu_0 H < 35$ mT in which the oscillations have nearly ideal periodicity. This fixes $\Delta B = 0.955$ mT.

Figure S7 compares the observed $\theta(H)$ (solid blue curve) with the ideal $\theta_0(B)$ (dashed line). The difference $\Delta\theta(H)$ (black curve) shows that, between 10 and 40 mT, the phase is nearly noise free aside from isolated phase jumps which are also evident in the raw curve of $\theta(H)$. The flatness of the profile of $\Delta\theta(H)$ in this interval implies that there is no accumulation (or loss) of phase winding arising from noise. Hence it provides a quantitative measure of the phase noise content in a specific interval. Starting at 60 mT, however, $\Delta\theta(H)$ increases steeply. This reflects crowding together of phase jumps as well as a slow variation of ΔB with H. The curve of $\Delta\theta(H)$ is reproduced in the main text (red curve in Fig. 2f).

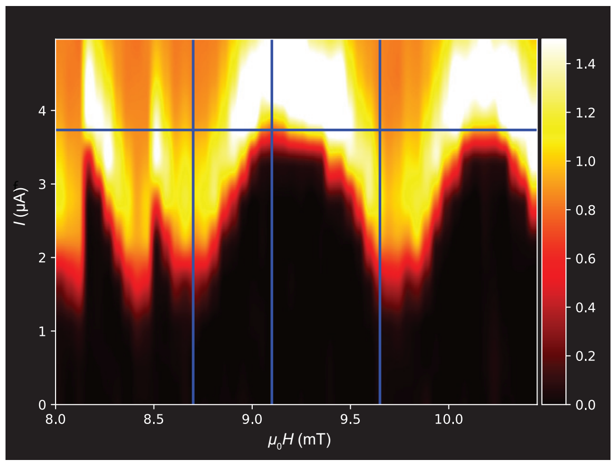

FIG. S6. A lobe from oscillation spectra of SA. The phases at the blue vertical lines (from left to right) are $\theta = \{2\pi(m-1), 2\pi(m-\frac{1}{2}), 2\pi m\}$, respectively.

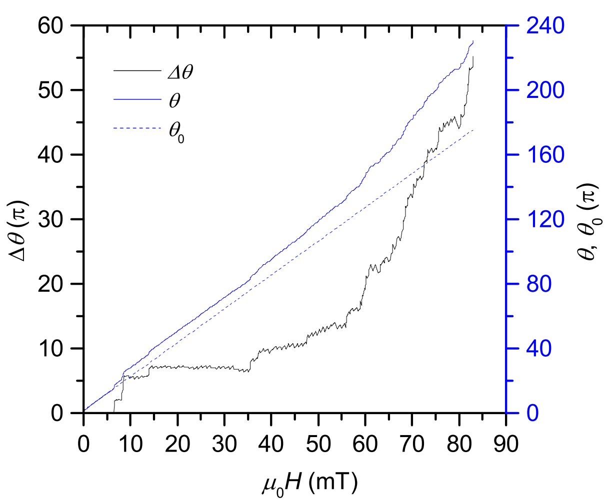

FIG. S7. Plot of the H dependence of the phase, $\theta(H)$, derived from the oscillations observed on an out-bound branch in device SA (solid blue curve). The ideal (noise-free) curve $\theta_0(H)$ is shown as a dashed line. The difference between $\theta(H)$ and $\theta_0(H)$ gives the difference $\Delta\theta(H)$ (black curve).

IV. COMPARISON WITH JOSEPHSON JUNCTION AND DC SQUID

We compare our experimental situation with the standard Josephson junction as well as a DC SQUID [7]. In our experiment the presence of two competing bulk pair fields and an edge supercurrent susceptible to either one requires a more elaborate analysis. Moreover, we have not used the Josephson supercurrent in our analysis. Nonetheless, phase winding caused by a weak field B underlies much of the physics here as well as in the 2 devices. Hence it is highly instructive to compare them.

In an SNS Josephson junction [7], a supercurrent $J_s = J_0 \sin\gamma(y)$ is injected $\parallel \hat{\mathbf{x}}$ into a normal metal N. A weak field $\mathbf{B} \parallel \hat{\mathbf{z}}$ induces winding of the phase $\gamma(y)$ of J_s along the transverse direction $\hat{\mathbf{y}}$ given by $\gamma(y) = \gamma(0) + 2\pi B(2\lambda + d)y/\phi_0$, where d is the junction length along $\hat{\mathbf{x}}$, $\phi_0 = h/2e$ is the superconducting flux quantum and λ is the penetration depth of H into the superconductors. The phase winding leads to a field profile for the observed current $I(B)$ described by Fraunhofer diffraction,

$$I(B) = bcJ_0 \sin\gamma(0)\frac{\sin(\pi\phi/\phi_0)}{\pi\phi/\phi_0}, \tag{S10}$$

where and b and c are the junction dimensions along the y and z axes, respectively, and the total flux $\phi = Bb(2\lambda + d)$. We emphasize that a pre-requisite for seeing the Fraunhofer diffraction is good uniformity of the phase-winding rate especially along x, typically achieved by having $d \ll b$ (see Ref. [1] for an experimental demonstration of how variation of contact geometry degrades and eventually suppresses altogether Fraunhofer diffraction in a series of junctions based on $MoTe_2$).

The inverse Fourier transform of $I_c(B)$ yields a supercurrent density $J_s(y)$ that is nearly uniform (independent of y). When edge supercurrents are dominant, there is no central peak. Instead, the observed $I_c(B)$ displays an oscillatory pattern analogous to a multi-slit diffraction pattern. Its Fourier transform yields a supercurrent distribution $J_s(y)$ comprised of two delta functions centred at the edges.

In our experiment the observed profile $I_c(B)$ looks incongrously like a superposition of the two limits (we first disregard the anti-hysteresis). We have a narrow central peak co-existing with densely spaced oscillation peaks. Although the regularity of the oscillations (on the out-bound branch) is consistent with edge supercurrents, the narrow central peak is inconsistent with a Fraunhofer maximum. One of our main conclusions is that the central peak is actually not a Fraunhofer diffraction effect. The strong competition evidenced by the stochastic swithching in Fig. 2 (main text) implies that the phase γ is never uniform in the bulk. Experimentlally, we find that the width of the central peak is nominally unchanged even when the contact sizes and geometries are varied greatly across devices. In particular, there should be no Fraunhofer diffraction in devices with very small Nb contacts (Samples SH and SD), yet their central peaks are similar to those in SA and SB. We reason that the central peak instead originates from proximitization of the bulk states by Nb. Hence its width reflects the critical field for suppressing this paired state, rather than the width of the Fraunhofer diffraction maximum.

Experimentally, the dominant role of hysteretic effects precludes standard Fourier analysis of the observed oscillations because the inbound and out-bound branches are radically distinct. One cannot Fourier transform one branch while discarding the other because both are needed to describe the blocade mechanism discussed in the main text.

If we regard the links ℓ_1 and ℓ_2 as weak links, a similarity with a double-junction DC SQUID device suggests itself. However, in the DC SQUID, the enclosed area is an inert vacuum. Here the enclosed area is comprised of bulk states that host the intrinsic and injected condensates. The set of phenomena observed – competition leading to stochastic switching, antihysteresis in the central peak and $(dV/dI)_0$, and the phase noise on in-bound branch – result from interactions between the bulk and edge states. They are absent in conventional DC SQUID devices.

V. MEASUREMENTS ABOVE T_c

As reported in the main text, we have found that an edge supercurrent can be induced by the pair field $\hat{\eta}$ injected from Nb even when the intrinsic pair field $\hat{\psi}$ is severly weakened by raising T well above T_c (100 mK). Superconductivity in the Nb contacts remains robust because of its critical temperature $T_{\mathrm{c,\ Nb}} \sim 8$ K. In Fig. 6c and 6d (main text) the edge supercurrent proximitized by $\hat{\eta}$ is observable as periodic (dissipationless) lobes in the color map of (dV/dI) at $T = 378$ and 722 mK (Sample SA). At both T, the phase noise is much reduced compared with corresponding maps at 18 mK. Importantly, the noise asymmetry between inbound and outbound branches is also considerably reduced as well. This is consistent with the inference that the large phase noise results directly from competition between the pair fields $\hat{\eta}$ and $\hat{\psi}$ to pair the edge states.

As noted, the competing effects are also evident in the antihysteretic curves of the zero-bias differential resistance $(dV/dI)_0$ as H is cycled between ± 100 mT. We show these curves at these elevated temperatures. At $T = 378$ mK (Fig. S8a), the onset field for dissipationless flow on the inbound branch (blue trace) is decreased to -20 mT (compared with -58 mT at 18 mK) whereas the return to dissipative flow on the outbound branch (red) is $\sim$4 mT (compared with 28 mT at 18 mK). Despite having T well above T_c, the edge oscillations are clearly observed as dense arrays of periodic narrow spikes that extend to ± 100 mT on both branches. A second feature is the persistence of the antihysteresis (green arrows). From both features, we infer that the amplitude $|\hat{\Psi}|$ remains finite in the vortex liquid state at 378 mK. The corresponding traces of $(dV/dI)_0$ at the higher temperature 722 mK are shown in Fig. S8b. At such a high T, both the edge oscillations and antihysteresis are strongly suppressed (but still detectable).

VI. PAIR FIELD, JOSEPHSON SUPERCURRENT AND PROXIMITY EFFECT

A. Pair field

In the main text, we frequently referred to the pair field. Here we review briefly its formulation. In the pairing model, the reduced BCS Hamiltonian is [7, 8]

$$\mathcal{H}_{pair} = 2\sum_{\mathbf{k}}(\epsilon_{\mathbf{k}} - \mu)c^{\dagger}_{\mathbf{k}\uparrow}c_{\mathbf{k}\uparrow} - \sum_{\mathbf{k},\mathbf{q}} V_{\mathbf{kq}}\left[b^{\dagger}_{\mathbf{k}}b_{\mathbf{q}} + h.c.\right], \tag{S11}$$

where $c^{\dagger}_{\mathbf{k}\uparrow}$ creates an electron in state $\mathbf{k}\uparrow$ of energy $\epsilon_{\mathbf{k}}$. The pair operator $b^{\dagger}_{\mathbf{k}} \equiv c^{\dagger}_{\mathbf{k}\uparrow}c^{\dagger}_{-\mathbf{k}\downarrow}$ creates a pair of electrons occupying $(\mathbf{k}\uparrow, -\mathbf{k}\downarrow)$. In both sums, we let $\mathbf{k}$ run over the entire Fermi surface, and associate spin $\uparrow$ and $\downarrow$ with $\mathbf{k}$ and $-\mathbf{k}$, respectively. The interaction term $V_{\mathbf{kq}}$ is the amplitude for scattering between the pairs indexed by $\mathbf{k}$ and $\mathbf{q}$. After Gor'kov factorization, we have $\langle b^{\dagger}_{\mathbf{k}}b_{\mathbf{q}}\rangle \simeq \langle b_{\mathbf{k}}\rangle^{*}b_{\mathbf{q}} + \langle b_{\mathbf{k}}\rangle b^{\dagger}_{\mathbf{q}}$, where $\langle\cdots\rangle$ is the expectation value (or

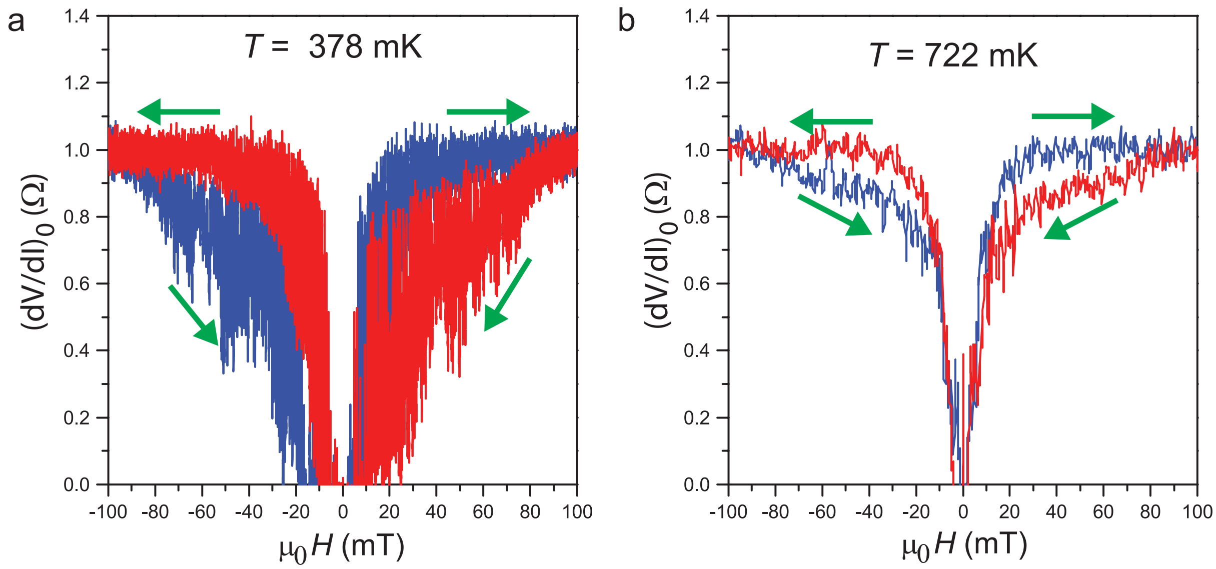

FIG. S8. Plots of the zero-bias differential resistance $(dV/dI)_0$ as H is cycled between ±100 mT in device SA at T = 378 (Panel a) mK and T = 722 mK (Panel b). The dense hash in Panel a is resolved as periodic oscillations caused by fluxoid quantization. The step size in field is 10× smaller in Panel a (ΔH = 0.1 mT) than in Panel b (1 mT). Green arrows indicate the field scan direction.

field amplitude) in the self-consistent field approach. The interaction part of Eq. S11 may then be expressed as

$$\mathcal{H}_{int} = -\sum_{\mathbf{q}} \left(\hat{\psi}^*_{\mathbf{q}} b_{\mathbf{q}} + \hat{\psi}_{\mathbf{q}} b^{\dagger}_{\mathbf{q}} \right), \tag{S12}$$

where $\hat{\psi}_{\mathbf{q}}$ is the (intrinsic) pair field that attempts to "align" the pair operators $b_{\mathbf{q}}$ given by

$$\hat{\psi}_{\mathbf{q}} = \sum_{\mathbf{k}} V_{\mathbf{kq}} \langle b_{\mathbf{k}} \rangle. \tag{S13}$$

An equivalent formulation of the pair field is given by Anderson's pseudospin picture [9]. For the $s = \frac{1}{2}$ pseudospin $\mathbf{s_k}$, the spin-up state $|\uparrow\rangle = (1,0)^{\mathrm{T}}$ corresponds to having both states $(\mathbf{k}\uparrow, -\mathbf{k}\downarrow)$ unoccupied whereas both states are filled in the spin-down state $|\downarrow\rangle = (0,1)^{\mathrm{T}}$ (quasiparticles are assumed absent). Expressing the pair creation operator as the spin-lowering operator $b^{\dagger}_{\mathbf{k}} = s^-_{\mathbf{k}} = s^x_{\mathbf{k}} - i s^y_{\mathbf{k}}$, we have for the interaction part of Eq. S11

$$\mathcal{H}_{int} = -2 \sum_{\mathbf{k},\mathbf{q}} V_{\mathbf{kq}} \left(\langle s^x_{\mathbf{k}} \rangle s^x_{\mathbf{q}} + \langle s^y_{\mathbf{k}} \rangle s^y_{\mathbf{q}} \right). \tag{S14}$$

This may be written as the dot product of $\mathbf{s_k}$ and a transverse field $\mathbf{H}_{\mathbf{k}\perp} = 2\sum_{\mathbf{q}} V_{\mathbf{kq}} \langle \mathbf{s}_{\perp\mathbf{q}} \rangle$, namely

$$\mathcal{H}_{int} = -\sum_{\mathbf{k}} \mathbf{H}_{\mathbf{k}\perp} \cdot \mathbf{s_k}. \tag{S15}$$

The transverse field $\mathbf{H}_{\mathbf{k}\perp}$ is equivalent to $\hat{\psi}_{\mathbf{k}}$ in Eq. S13.

In our experiment, supercurrent injected from Nb introduces a pair field $\mathbf{H}_{\mathbf{k}\perp}$ that is incompatible with the intrinsic pair field of $MoTe_2$.

B. Josephson current in unconventional superconductors

Early experiments testing incompatibility between conventional and unconventional superconductors looked for a Josephson supercurrent in Nb point contacts pressed against candidate unconventional superconductors. While our experiment does not utilize point contacts or the Josephson supercurrent, it is helpful to survey the pitfalls and ensuing complications in experiments based on the Josephson effect in point contact junctions.

Pals *et al.* [11] initially proposed that pair tunneling should be absent between singlet and triplet superconductors. Han *et al.* [13] investigated the Josephson supercurrent between a Nb point contact and the surface of heavy fermion (HF) superconductors UBe_{13} (with $T_c =$ 0.85 K), $LaBe_{13}$ (0.45 K) and $CeCu_2Si_2$ (0.6 K). In the presence of microwave radiation (25 GHz), they observed the emergence of Shapiro steps over a broad range of T (1.2– 4.2 K) well above the T_c of the HF superconductor. They proposed that Josephson tunneling occurs between Nb and a thin layer of HF proximitized by Nb above its T_c. The proximity-induced Josephson tunneling (PJIT) has drawn considerable attention and discussion.

Applying the correlation-function method near T_c, Fenton [10] obtained results that strongly challenged the expectation that the Josephson effect may provide a simple yes/no litmus test for unconventional superconductivity. Fenton found that strong spin-orbit coupling combined with small HF pair size can lead to admixing of singlet and triplet states at the boundary.

Yip *et al.* [4] used the Ginzburg-Landau approach to investigate Josephson tunneling between a conventional and an unconventional superconductor. They employed both spatial symmetry and time-reversal invariance constraints to see which terms are forbidden. Addressing the possibility of PJIT, they conclude that dissipationless tunelling above T_c of the HF supercondutor can be ruled out.

C. Quasiclassical calculations of the proximity effect

Modern treatments of the proximity effect mostly utilize the quasiclassical method in which the large-momentum components of all Green's function propagators are integrated over. At the interface between different superconductors, the boundary condition matching is applied only to the resulting envelope functions.

Ashauer, Kieselmann and Rainer [2] have applied the quasiclassical approach to investigate the proximity effect between a clean, very thin s-wave superconductor in proximity contact with a bulk p-wave superconductor. With the latter in the Anderson Brinkman Morel state, they found that the critical temperture T_c of the s-wave film is suppressed precipitously to zero when the rescaled thickness $\bar{a} = a/(1-R)$ is decreased below the coherence length $\xi_0 = \hbar v_F/(2\pi k T_c^0)$ (a is the film thickness and R the reflection coefficient). Interestingly, the T_c suppression is almost identical to that induced by a bulk normal metal. Next, assuming that the bulk is in the isotropic Balian-Werthamer state, they also found that the thin-film s-wave order parameter Δ_s is strongly depressed at the interface. The suppression is similar in magnitude if the bulk is a normal metal. On the bulk side, the p-wave order parameter also suffers a strong suppression with decay (Pippard) length $\xi_s = \hbar v_F/(2\Delta_s)$, especially for momenta perpendicular to the interface. Hence, incompatible order parameters mutually suppress each other's order parameter at the interface on a length scale close to the Pippard length.

Using the quasiclassical method, Thuneberg and Ambegaokar [3] showed that, close to T_c, the GL form often adopted to describe Josephson tunneling in a point contact can be obtained. They addressed the PJIT effect by modelling the point contact as a thin, weakly proximitized layer S sandwiched between a normal metal N (the HF above its T_c) and a strong superconductor S' (Nb). They obtain a Josephson supercurrent that varies as $\sin 2\phi$. The frequency doubling arises because the amplitude A of the induced gap in S varies as $\cos\phi$ so that $J_s \sim \cos\phi \sin\phi$.

Microscopic calculations have largely confirmed Fenton's finding that strong spin-orbit coupling and magnetically active interfaces can render the Josephson effect test invalid. Several groups have shown that a Josephson current can arise from spin-orbit scattering of electrons at the interface between singlet and triplet superconductors. Millis, Rainer and Sauls [12] have carried out a detailed investigation of boundary conditions for superconductors across magnetically active interfaces, with application to possible HF superconductors. They discuss qualitative features of Josephson tunneling between conventional and HF superconductors.

Quasiclassical calculations do not appear to have been carried out for superconductors bearing edge states. Hopefully, our findings will motivate these calculations.

[1] Wudi Wang, Stephan Kim, Minhao Liu, F. A. Cevallos, R. J. Cava, and N. P. Ong, Evidence for an edge supercurrent in the Weyl superconductor $MoTe_2$, *Science* **368**, 534-537 (2020). 10.1126/science.aaw9270

[2] B. Ashauer, G. Kieselmann and D. Rainer, On the proximity effect in unconventional superconductors, *J. Low Temp. Phys.* **63**, 349 (1986).

[3] E. V. Thuneberg and Vinay Ambegaokar, Microscopic theory of the proximity-induced Josephson Effect, Phys. Rev. Lett.**60**, 365 (1988).

[4] S. K. Yip, O. F. De Alcantara Bonfim and P. Kumar, Supercurrent tunneling between conventional and unconventional superconductors: a Ginzburg-Landau approach, Phys. Rev. B**41**, 11214 (1990).

[5] Manfred Sigrist and Kazuo Ueda, Phenomenological theory of unconventional superconductivity, *Rev. Mod. Phys.* **63**, 23 (1991).

[6] Zheyi Zhu, Stephan Kim, Shiming Lei, Leslie M. Schoop, R. J. Cava, and N. P. Ong, Phase tuning of multiple Andreev reflections of Dirac fermions and the Josephson supercurrent in Al-$MoTe_2$-Al junctions, *Proc. Nat. Acad. Sci.*, *in press.*

[7] M. Tinkham, *Introduction to Superconductivity* (Dover, New York, 2004), Ch. 6.

[8] J. R. Schrieffer, *Theory of Superconductivity* (Addison Wesley, 1988), Ch. 2.

[9] P. W. Anderson, Random-phase approximation in the theory of superconductivity, *Phys. Rev.* **112**, 1900 (1958).

[10] E. W. Fenton, Proximity and Josephson effects for heavy-fermion superconductors, *Sol. State Commun.* **54**, 709-713 (1985).

[11] J. A. Pals, W. van Haeringen and M. H. van Maaren, Phys. Rev. B**15**, 2592 (1977).

[12] A. J. Millis, Proximity effects between singlet and triplet superconductors, Physica **135B**, 69–71 (1985).

[13] S. Han, K. W. Ng, E. L. Wolf, H. F. Braun, L. Tanner, Z. Fisk, J. L. Smith, and M.R. Beasley, Phys. Rev. B**32**, 7567 (1985).